Study of $K^{\pm}\pi^{\mp}$, $K^{+}K^{-}$ and $K^{-}p$ Production in DIRAC Using Time-of-Flight Measurements

B. Adeva[1], A. Romero[1], O. Vázquez Doce[1,2], C. Mariñas[1], J.L. Fungueiriño[1]

[1] *IGFAE, University of Santiago de Compostela, Spain*

[2] *INFN, Istituto Nazionale di Fisica Nucleare, Frascati, Italy*

Abstract

Two separate experimental studies are presented in this note, concerning the pair momentum dependence of the ratios $K^{\pm}\pi^{\mp}/\pi^{+}\pi^{-}$ and $K^{+}K^{-}/\pi^{+}\pi^{-}$. Only time-of-flight measurements are used in DIRAC, from both the Vertical Hodoscopes and the upstream detectors. In the first case, the full 2001 p-Ni data sample is used, with normal triggers. For the latter, all Lambda triggers from 2001, 2002 and 2003 are employed in order to reach access to $K^{\pm}$ identification at high momentum. An extensive comparison with UrQMD Monte Carlo is performed, particularly concerning the momentum derivative.

DIRAC note 2007-02 *19 February 2007*

1 Analysis of momentum dependence of $K^{\pm}\pi^{\mp}/\pi^{+}\pi^{-}$ from time difference between the two arms in VH

In order to understand the physics of strangeness production in proton-Ni collisions in DIRAC (at 24 GeV/c proton momentum), particularly in 2001 data runs, we have determined the momentum dependence of the observed $K^{+}\pi^{-}$ and $K^{-}\pi^{+}$ signals, normalized to the semi-inclusive $\pi^{+}\pi^{-}$ production. The results obtained were compared with the UrQMD Monte Carlo [1], with special emphasis in checking whether the momentum derivative is correctly described by this relativistic model. In the following, we shall denote these by ratios $r_K^{+} = K^{+}\pi^{-}/\pi^{+}\pi^{-}$ and $r_K^{-} = K^{-}\pi^{+}/\pi^{+}\pi^{-}$.

The TOF detector (Vertical Hodoscopes) is sufficiently precise to provide a clear $K^{\pm}$ signal from the time difference $\Delta t = t_{-} - t_{+}$ between the two hodoscopes [2], once the pion mass hypothesis is made in the $(\mp)$ arm, opposite to the charged kaon under search. The best K^{+} signal analysis is provided by the invariant mass squared, according to the expression:

$$M_{+}^{2} = p_{+}^{2}\left[\left(\frac{L_{-}}{L_{+}}\sqrt{1+\frac{M_{\pi}^{2}}{p_{-}^{2}}}-\frac{c\Delta t}{L_{+}}\right)^{2}-1\right] \qquad (1)$$

and similarly M_{-}^{2} for K^{-}, after overall sign flipping in the above expression. $L_{\pm}$ and $p_{\pm}$ are the respective pathlengths and momenta, in each arm. Invariant mass resolution degrades with increasing momentum of the analized particle $p_{\pm}$, which is equivalent to increasing momentum of the sum $p = p_{+} + p_{-}$, given the fact that the trigger structure makes positive and negative momenta nearly equal. We have analized both the positive and negative kaon mass spectra in 11 $200MeV/c$ bins of the pair momentum p, as it is shown in Figs. 1 to 11. It can be appreciated that mass resolution is still good enough up to pair momenta of 5.0 GeV/c. Guided by the observed spectra, we have parametrized the signals by a two-gaussian fit added to a polynomial background, for each momentum bin. The $\pi^{+}\pi^{-}$ signal (which is observed at M_{π}^{2}), was also analysed in this way, using the same two-gaussian parametrization as for the $K^{\pm}\pi^{\mp}$ signal, as expected from the approximately equal resolution. The ratio r_K^{+-} found after background subtraction at each momentum bin, is displayed in Fig. 12 as function of pair momentum p. The analysis shown in the previous figures includes the full Ni 2001 data sample, with normal physics runs, as it was used for Pionium lifetime analysis [4]. In the 3 lowest momentum bins the statistical errors were slightly increased (by factors 2.5,2.3 and 1.8 for K^{-} and 2.0,1.9 and 1.2 for K^{+}), in order to cope with a small systematic discrepancy with respect to the parametrization at the left side of both the $K^{+}\pi^{-}$ and

$K^-\pi^+$ signals, nearly invisible in the figures. Such increase was not needed in the other bins, the χ^2 values being excellent in all cases.

Fig. 12 shows a clear rise of both r_K^+ and r_K^- ratios as function of momentum. In addition, the K^+ signal is very significantly larger than the K^-, by a factor 2.75 on average. We have studied whether this behaviour can be understood by the strangeness production model in the UrQMD Monte Carlo, and for that purpose we evaluated both the physics output of the model, as well as the DIRAC spectrometer efficiency, particularly important because of the $K^\pm$ longer lifetime as compared to $\pi^+\pi-$.

This was done in two steps:

a) 2049 million pNi events were generated at proton momentum 24 GeV/c (using UrQMD version 1.3) and all $K^+\pi^-$, $K^-\pi^+$ and $\pi^+\pi^-$ pair combinations were selected in the final state, after requiring $4.5^o < \theta < 7.0^o$ where θ is the angle between the vector sum of the particle momenta and the incoming proton direction. The ratios $K^+\pi^-/\pi^+\pi^-$ and $K^-\pi^+/\pi^+\pi^-$ are plotted as function of pair momentum p in Fig. 12. A cut $Q < 30MeV/c$ was applied to the center-of-mass momentum Q, calculated in the $\pi^+\pi^-$ hypothesis irrespective of particle masses. An additional momentum cut 1.3 $GeV/c < p_{+-} < 5.0$ GeV/c was applied for each track.

The UrQMD time parameter [1], which governs the hadron physics, was fixed to $t = 20fm/c$. In order to take into account the contribution of weak decays into both $K^\pm$ and $\pi^\pm$, we have implemented an interface with the PHYTIA/JETSET program by which mesons and baryons are weakly decayed. The correction with respect to the undecayed spectra is small (aproximately 5%).

b) in order to evaluate the spectrometer efficiency, we generated π^+K^- events using the standard DIRAC generator for Coulomb pairs (including the correct Coulomb factor with $K\pi$ Bohr momentum) and processed them first through the GEANT-DIRAC interface with the correct particle asignment (lifetime in particular), and later reconstructed them with the same version of the ARIANE program as it was used for the experimental data, under the cuts $Q_L < 22MeV/c$ (of course calculated in $\pi^+\pi^-$ hypothesis) and $Q_T < 5MeV/c$. The momentum spectrum of reconstructed $K^\pm\pi^\mp$ events was determined, and divided by that of the generated events, in order to determine the spectrometer acceptance efficiency function. The same operation was done for $\pi^+\pi^-$ pairs, using this time the standard Monte Carlo production chain. It was noted that in the central momentum region (unaffected by edge effects) the $K^+\pi^-$ spectrometer acceptance had a steeper momentum dependence than it had for $\pi^+\pi^-$, as expected from the longer K^+ lifetime. What we are interested

in is the ratio between $K^{\pm}\pi^{\mp}$ and $\pi^{+}\pi^{-}$ efficiency functions. This function is actually the same, for both $K^{\pm}$ charge modes.

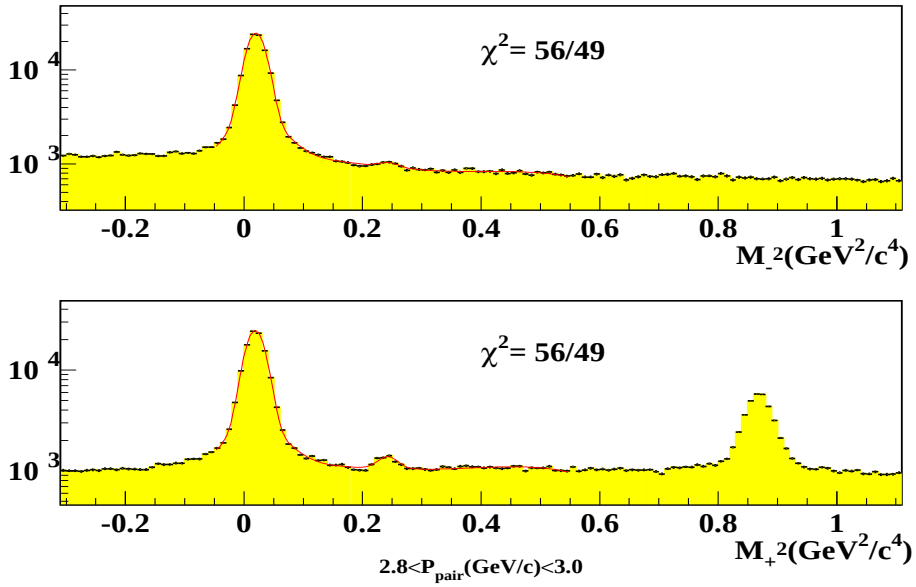

Fig. 1. *Spectrum of squared invariant mass of negative particle M_-^2 when pion mass is assumed in the opposite arm (top). The positive mass M_+^2 is also shown, with the corresponding hypothesis (bottom). Pair momentum interval as indicated. χ^2/ndf values are given for the fit described in the text.*

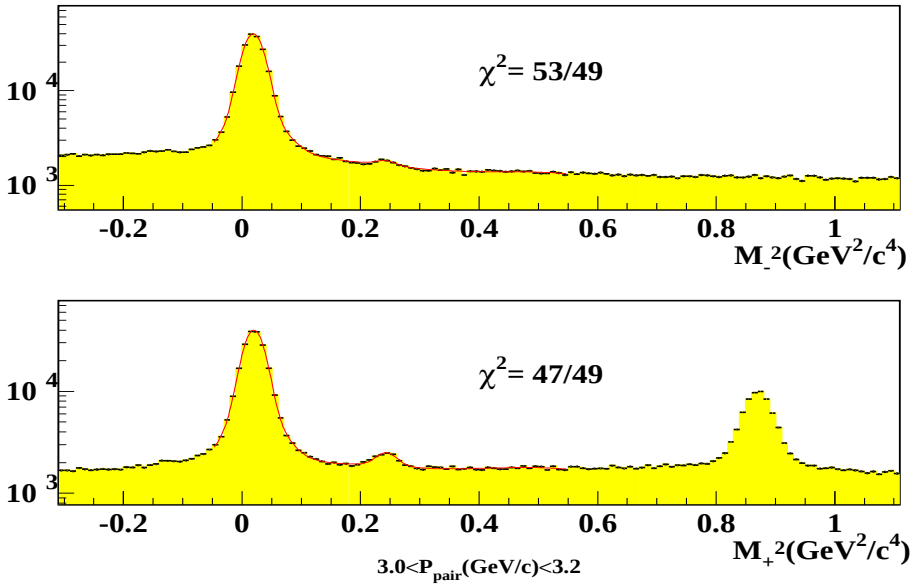

Fig. 2. *Spectrum of squared invariant mass of negative particle M_-^2 when pion mass is assumed in the opposite arm (top). The positive mass M_+^2 is also shown, with the corresponding hypothesis (bottom). Pair momentum interval as indicated.*

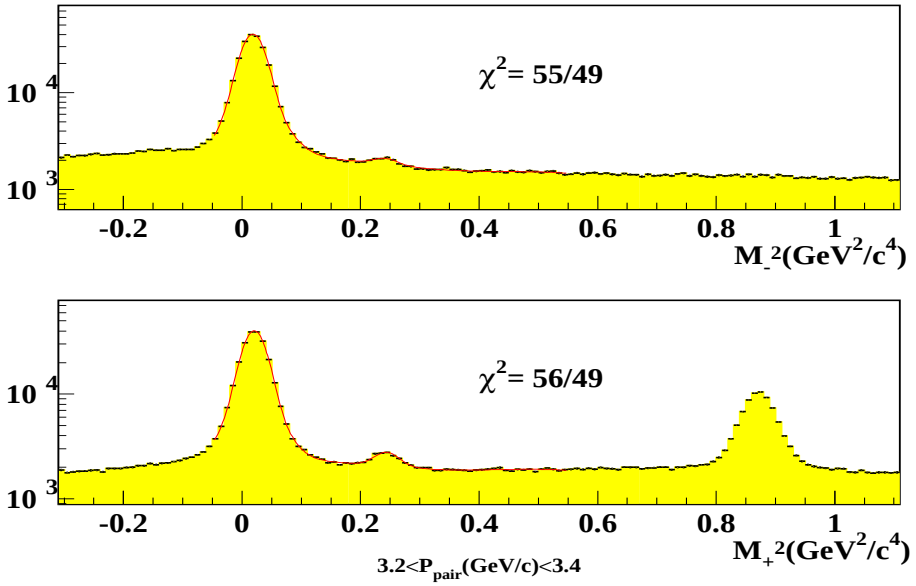

Fig. 3. *Spectrum of squared invariant mass of negative particle M_-^2 when pion mass is assumed in the opposite arm (top). The positive mass M_+^2 is also shown, with the corresponding hypothesis (bottom). Pair momentum interval as indicated.*

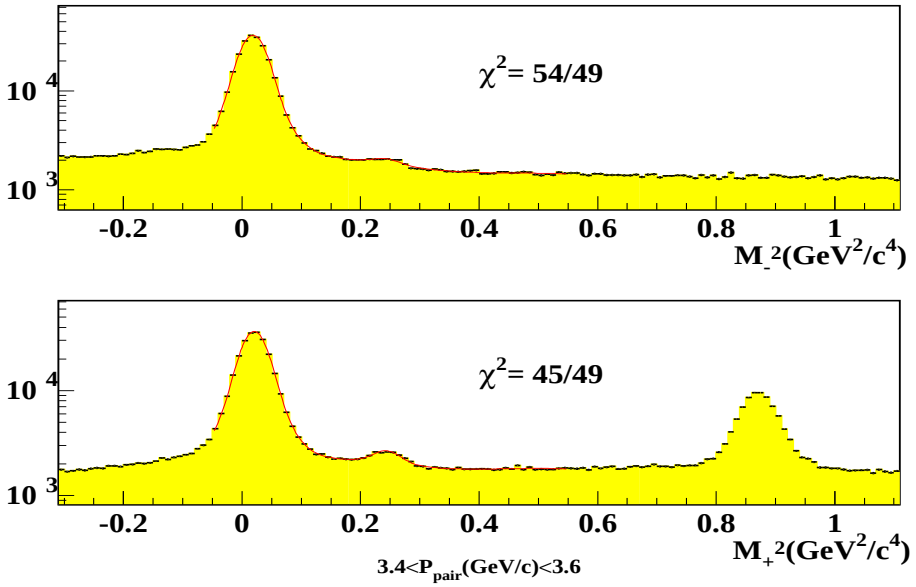

Fig. 4. *Spectrum of squared invariant mass of negative particle M_-^2 when pion mass is assumed in the opposite arm (top). The positive mass M_+^2 is also shown, with the corresponding hypothesis (bottom). Pair momentum interval as indicated.*

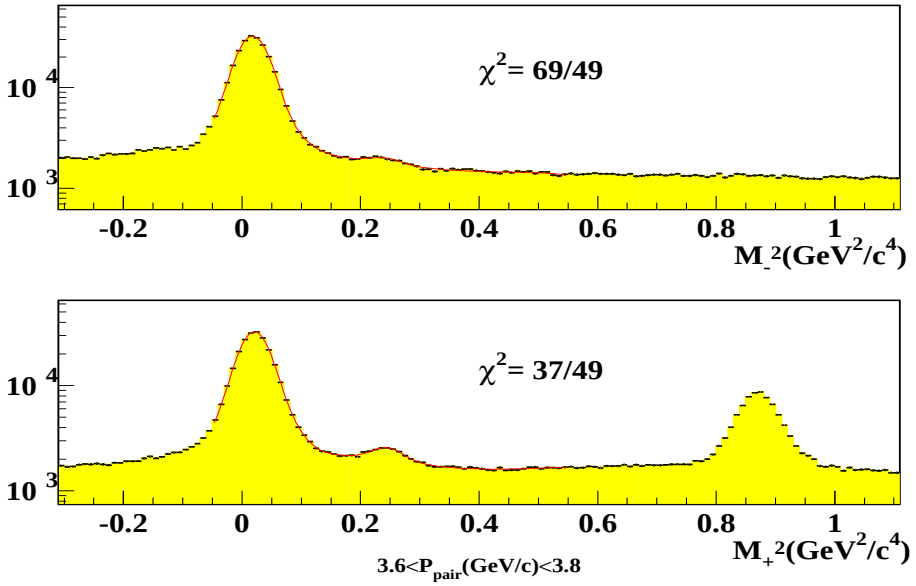

Fig. 5. *Spectrum of squared invariant mass of negative particle M_-^2 when pion mass is assumed in the opposite arm (top). The positive mass M_+^2 is also shown, with the corresponding hypothesis (bottom). Pair momentum interval as indicated.*

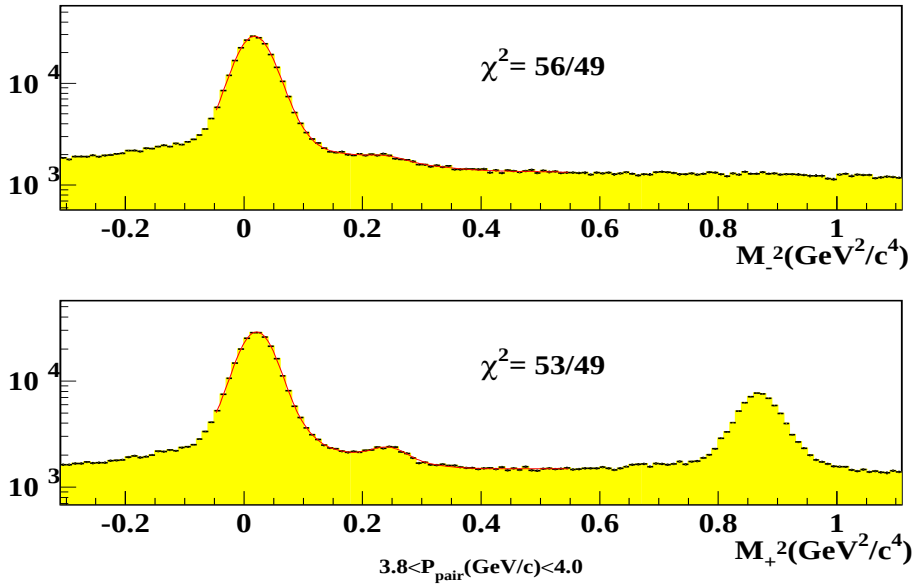

Fig. 6. *Spectrum of squared invariant mass of negative particle M_-^2 when pion mass is assumed in the opposite arm (top). The positive mass M_+^2 is also shown, with the corresponding hypothesis (bottom). Pair momentum interval as indicated.*

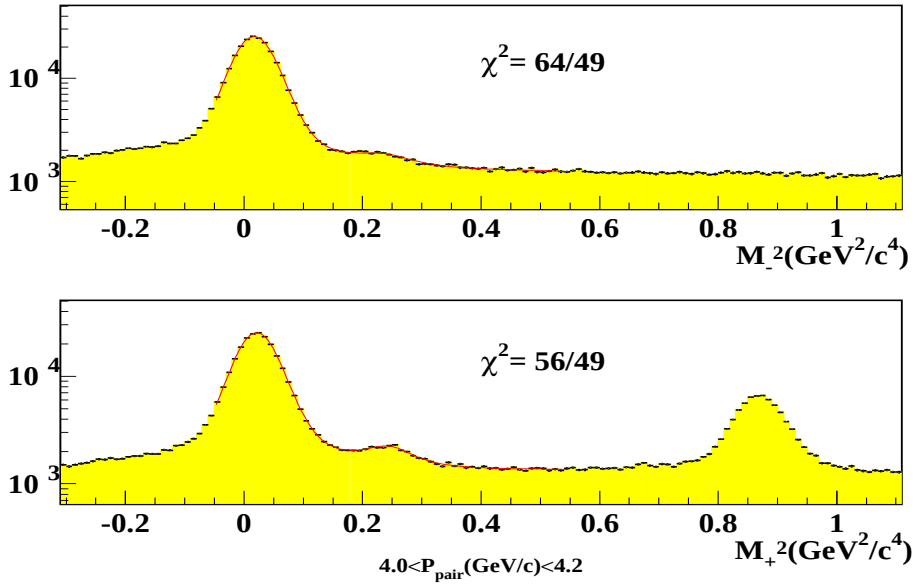

Fig. 7. *Spectrum of squared invariant mass of negative particle M_-^2 when pion mass is assumed in the opposite arm (top). The positive mass M_+^2 is also shown, with the corresponding hypothesis (bottom). Pair momentum interval as indicated.*

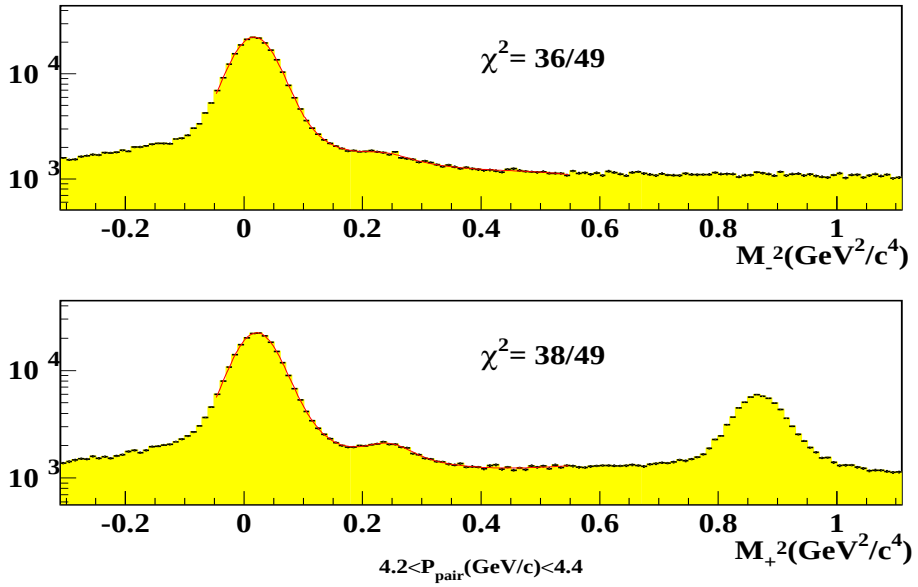

Fig. 8. *Spectrum of squared invariant mass of negative particle M_-^2 when pion mass is assumed in the opposite arm (top). The positive mass M_+^2 is also shown, with the corresponding hypothesis (bottom). Pair momentum interval as indicated.*

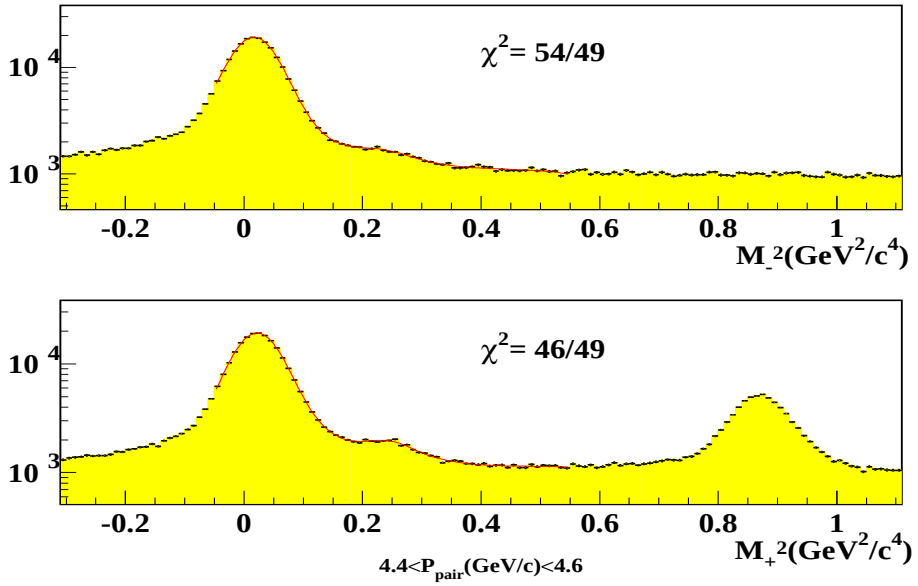

Fig. 9. *Spectrum of squared invariant mass of negative particle M_-^2 when pion mass is assumed in the opposite arm (top). The positive mass M_+^2 is also shown, with the corresponding hypothesis (bottom). Pair momentum interval as indicated.*

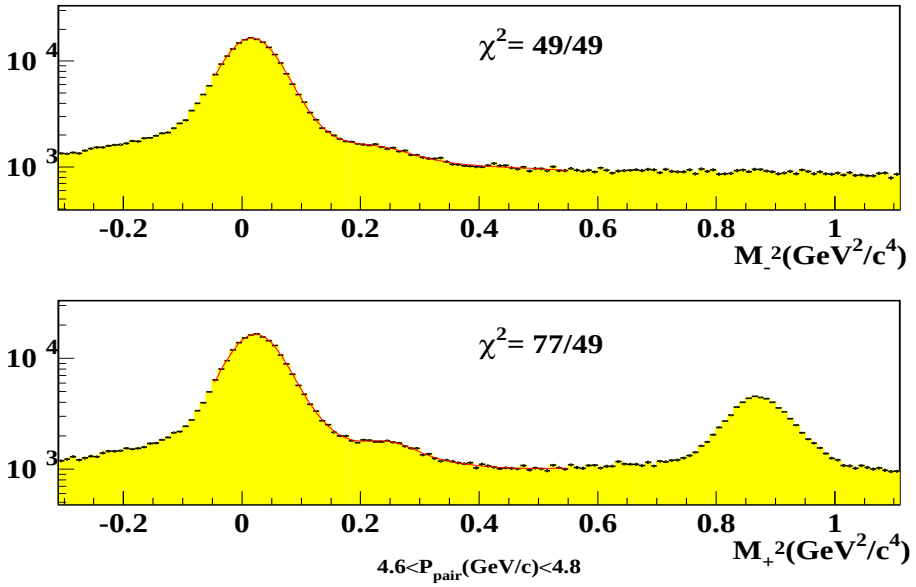

Fig. 10. *Spectrum of squared invariant mass of negative particle M_-^2 when pion mass is assumed in the opposite arm (top). The positive mass M_+^2 is also shown, with the corresponding hypothesis (bottom). Pair momentum interval as indicated.*

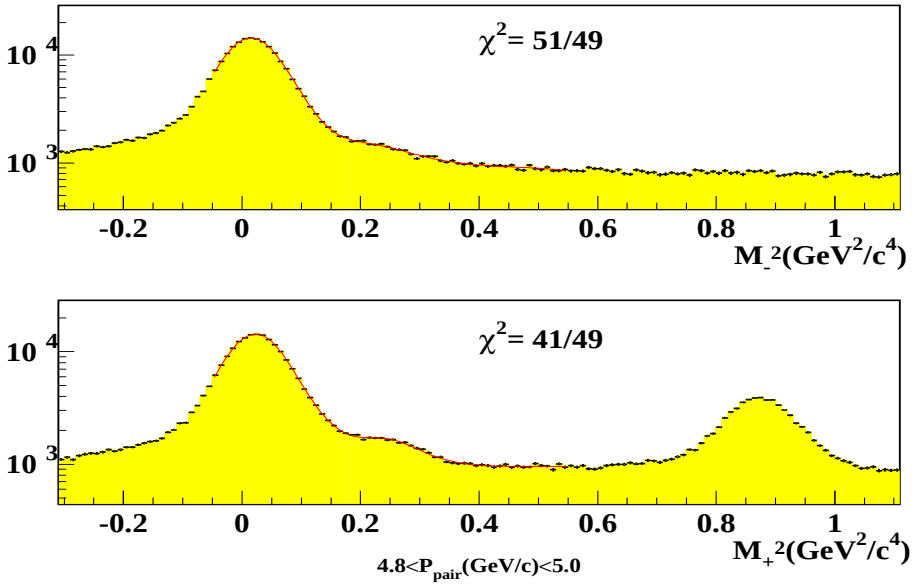

Fig. 11. *Spectrum of squared invariant mass of negative particle M_-^2 when pion mass is assumed in the opposite arm (top). The positive mass M_+^2 is also shown, with the corresponding hypothesis (bottom). Pair momentum interval as indicated.*

The r_K^{+-} spectra given by the UrQMD Monte Carlo physics at the generator level were multiplied by the efficiency function defined above, and the corrected function was compared with the experimental data in Fig. 12. In can be appreciated that the momentum derivative of the $K^{\pm}\pi^{\mp}/\pi^{+}\pi^{-}$ ratio is perfectly well described by UrQMD, for both charge signs in the analysed momentum range. However, the values of r_K^{+} and r_K^{-} ratios do not appear to be correctly described, since the Monte Carlo predictions had to be multiplied by factors 0.60 and 0.31, respectively, in order to find agreement with the experimental data. It seems that, whereas the strangeness momentum spectra are well described, the integrated production rates are not. In any case, the Monte Carlo predicts correctly a smaller $K^{-}\pi^{+}$ rate, as compared to $K^{+}\pi^{-}$.

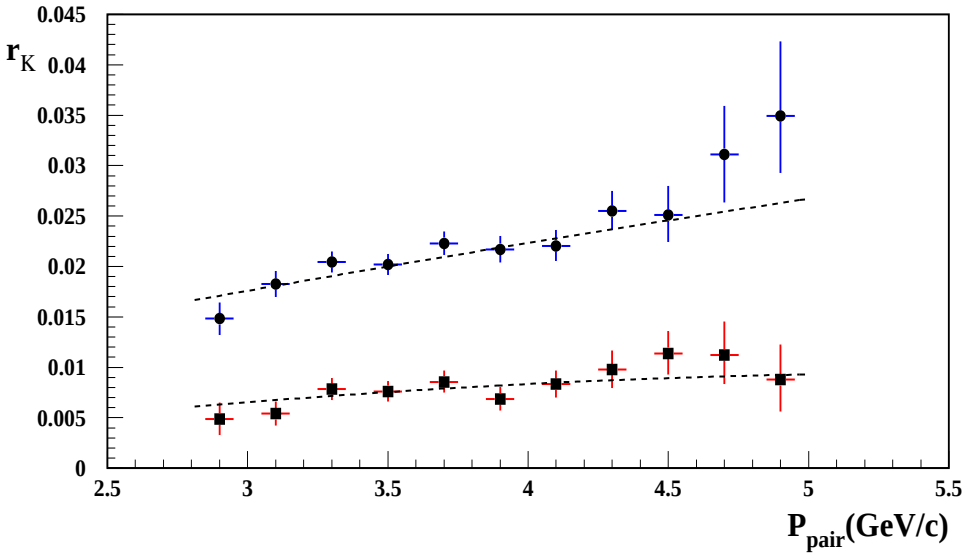

Fig. 12. *Momentum dependence of the measured ratios r_K^{+} (circles) and r_K^{-} (squares). The corresponding dotted lines indicate the acceptance corrected UrQMD Monte Carlo predictions, multiplied by factors 0.5 and 0.25 respectively.*

2 Analysis of $K^+K^-/\pi^+\pi^-$ at high momentum from utilization of asymmetric triggers

In a previous note [3] we have determined the $K^+K^-/\pi^+\pi^-$ ratio at $p = 2.9\ GeV/c$, using the full Ni 2001 data sample with the standard physics triggers used in Pionium analysis. Because of the low-Q (symmetric) trigger structure, the precision time-difference between vertical hodoscopes becomes useless for equal-mass pairs, and only the upstream time-of-flight measurements could be used succesfuly in that analysis. As a consequence, pair momentum was bound to be extremely low, thus providing no information on the momentum derivative.

The precise measurement of Pionionium lifetime [4] will require a small correction that takes into account the missidentified K^+K^- pairs in the $\pi^+\pi^-$ sample, and we need to know the yield and momentum dependence of this contamination, in order to evaluate the correction.

If we want to search for a K^+K^- signal at higher values of momentum, we need to go to asymmetric (unequal velocity) triggers. In this way, the precision time-difference between the two arms will become useful for mass discrimination. Fortunately the Lambda triggers are very well suited for the purpose [5],[6]. The only problem is statistics, since these triggers only occupy a small fraction of the normal DAQ runs. In order to cope with this, we have consistently integrated in our analysis all p-Ni data from 2001, 2002 and 2003 data taking periods.

As best discriminator to obtain the K^+K^- signal we define the *upstream mass squared*, asociated to a given upstream detector i, for positive (negative) particle as:

$$m^{2^i}{}_{+(-)} = p^2{}_{+(-)} \left[\left(\frac{\Delta t^i{}_{+(-)} c}{L^i{}_{+(-)}} \right)^2 - 1 \right] \tag{2}$$

where c is light velocity, $p_{+(-)}$ is the positive (negative) particle momentum, $\Delta t^i{}_{+(-)}$ is the delay between upstream detector i and VH for positive (negative) particle and $L^i{}_{+(-)}$ are the path lengths between detector i and VH. The upstream detectors are designated by $i = 1, ..., 4$ for IH [7] and $i = 5, 6$ for SFD (X and Y).

In addition we define, only for the positive particle, the *average* upstream mass squared:

$$m^2{}_+ = \frac{\Sigma m^{2i}{}_+}{N} \tag{3}$$

where the sum runs over the N upstream detectors involved. Only events whose negative track has hits in all upstream detectors are actually retained in the subsequent analysis.

We select events in the range $1.2\ GeV/c < p_- < 1.6\ GeV/c$ and $2.8\ GeV/c < p_+ < 4.0\ GeV/c$. Note that the positive particle average momentum is significantly higher than the negative one, due to the Lambda trigger structure (see [6] for more details).

The 6 experimental distributions obtained with $\pi^+\pi^-$ pairs for $m^{2i}{}_-$ as well as that for $m^2{}_+$ are very well described by the generic (asymmetric) parametrization:

$$R(x) = Ae^{-(a_1|x|^2 + a_2|x|^3 + a_3|x|^4)} \tag{4}$$

for $x \geq 0$ and $R(x) = Ae^{-(b_1|x|^2 + b_2|x|^3 + b_3|x|^4)}$ for $x \leq 0$, with $x = m^2 - m_0^2$, where m^2 is any of the upstream masses defined above and m_0^2 is an arbitrary parameter to locate the peak value. This parameter is set to the pion mass $m_0^2 = m_\pi^2$, but it can changed to other values, because m^2 resolution is weakly dependent on the mass scale. The a_i and b_i parameter values were determined independently in each case, and the fitted curves are shown in Fig. 13 for $m^2{}_+$ and Fig. 14 for $m^{2i}{}_-$. They represent the experimental resolution functions for each quantity. Note for example that the negative invariant mass resolution is better than the positive one, as it can be clearly appreciated from a comparison between the previous figures, as a consequence of the difference in momentum spectrum mentioned earlier.

Protons are removed by the cut $-0.2 < m^2{}_+(GeV^2/c^4) < 0.5$, whereas K^- identification is provided by requiring $0.015 < m^{2i}{}_-(GeV^2/c^4) < 0.44$ for all upstream detectors $i = 1, 6$ [1]. These cuts play the role of a very strong pion veto, based upon the upstream time-of-flight measurements only. Their effect is illustrated in Figs. 13 and 14 by showing as shaded area the event fractions retained in each case.

After the background suppression provided by the above cuts, we are now in position to analize the fine structure of the spectrum of the negative mass

[1] except for $IH - B$ where the upper limit was $0.7\ GeV^2/c^4$ (see Fig. 14).

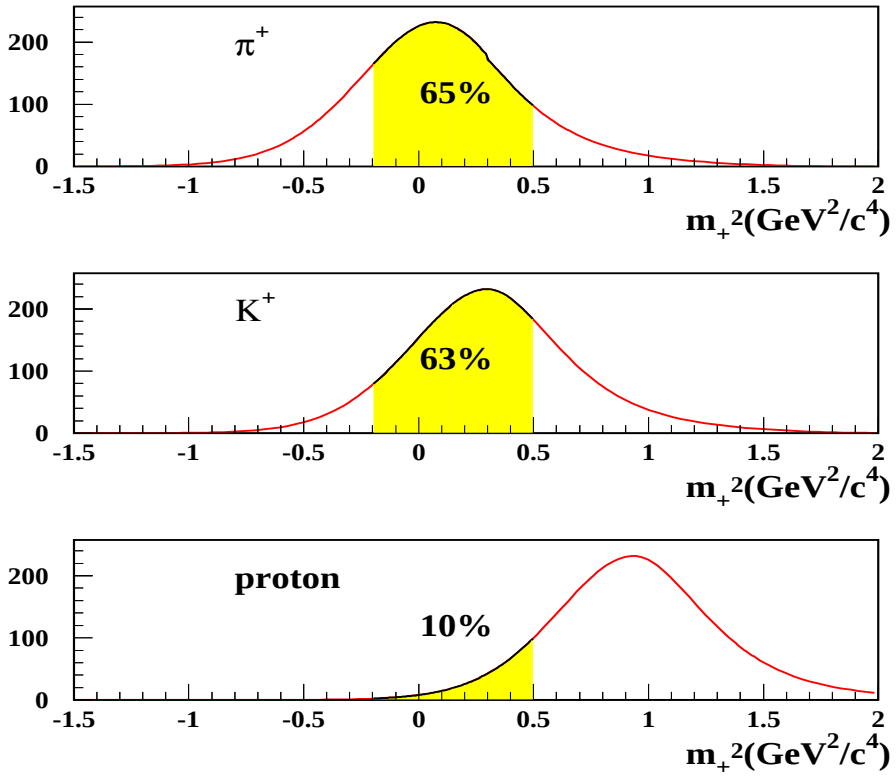

Fig. 13. *Resolution function for the positive upstream squared mass m_+^2, obtained from a parametrization fitted to the experimental $\pi^+\pi^-$ data. The peak value has been displaced to three different mass hypothesis, in order to appreciate the effect of the cuts described in the text.*

Table 1
Efficiency implied by upstream positive mass cuts.

Particle	Efficiency(%)
π^+	65
K^+	63
proton	10

$M^2{}_-$, defined from the precision time-difference in the Vertical Hodoscopes, which is given by:

$$M_-^2 = p_-^2 \left[\left(\frac{L_+}{L_-} \sqrt{1 + \frac{M_K^2}{p_+^2}} - \frac{c\Delta t}{L_-} \right)^2 - 1 \right] \qquad (5)$$

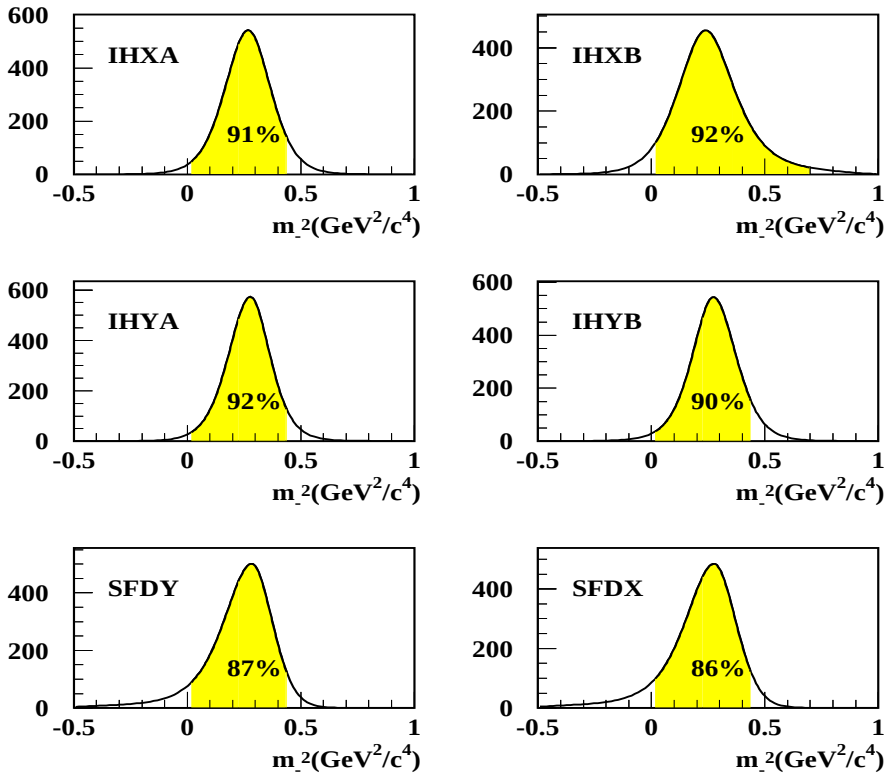

Fig. 14. *Negative upstream mass resolution functions, obtained for each of the 6 Ionization Hodoscope (IH) detectors, obtained from parametrizations fitted to the experimental $\pi^+\pi^-$ data. The peak values were centered at M_K^2, in order to illustrate the effect of the cuts given in the text for K^- selection.*

following the same notation as previuosly used for expression (1), with the remark that the K^+ hipothesis in the opposite arm has now been chosen. The spectrum with full statistics is shown in figure 15, where four enhancements can be observed, which we attribute in principle to $\pi^+\pi^-$, K^-p, K^+K^-, and π^+K^- production. Please note that only the K^+K^- signal is seen at the correct mass hypothesis ($M_-^2 = M_K^2$), the others being shifted according to predictable deviations due to the positive particle time slewing. A more detailed analysis of this particular spectrum shows that the second peak is actually dominated by a background originated from a reflection of the negative upstream mass cuts, as we will see below, and that this is the reason for its broader structure.

Table 2
Implied efficiency values for each upstream detector mass cuts.

Detector	Efficiency(%)
IHXA	91
IHXB	92
IHYA	92
IHYB	90
SFDY	87
SFDX	86
Total	54

The signal yield is analized by maximization of the following likelyhood function:

$$L(x) = \sum_{\alpha=1}^{3} A_\alpha G_\alpha(x - x_{0\alpha}, \sigma_\alpha) + A_b G_b(x - x_{0b}, \sigma_b) + B P_4(x) \qquad (6)$$

where $x = M_-^2$ and $G_\alpha(x)$ represent normalized gaussian functions with peak value at $x = x_{0\alpha}$ and width σ_α describing the $\pi^+\pi^-$, K^+K^- and π^+K^- signals for $\alpha = 1, 2, 3$, respectively. Similarly $G_b(x)$ is a gaussian describing the background broad structure in the neibourghood of the K^-p signal. An additional smooth background is described by the normalized fourth order polynomial $P_4(x) = (1+\sum_{i=1}^{4} c_i x^i)/I_4$ where $I_4 = \int_{x_1}^{x_2}(1+\sum_{i=1}^{4} c_i x^i)dx$ is the normalization integral. The signal event rates are then provided by the coefficients A_α.

The parameters $x_{0\alpha}$,σ_2 and σ_3 were determined independently, and remained fixed in the fit procedure. The rest (σ_1,σ_b,A_α,A_b,B,c_i) were left free. The location of the $x_{0\alpha}$ peaks was determined by selecting signal events under the peak with the correct mass hypothesis and projecting them into the uncorrect hypothesis, in order to evaluate the mass shift.

Table 3 and Figure 15 show the fit results.

The number of K^+K^- pairs found by the fit are $N_{KK}^{obs} = 70^{+17}_{-16}$, and the total number of $\pi^+\pi^-$ pairs found when removing the $m_-^{2\ i}$ cuts is $N_{\pi\pi}^{obs} = 22942$. Both numbers need to be corrected for acceptance. The positive mass cut efficiency (see Fig. 13 top) is involved in the $\pi\pi$ case:

$$N_{\pi\pi} = N_{\pi\pi}^{obs} \times \frac{1}{Eff(\pi^+)} = 22942 \times \frac{1}{0.6514} = 35219 \qquad (7)$$

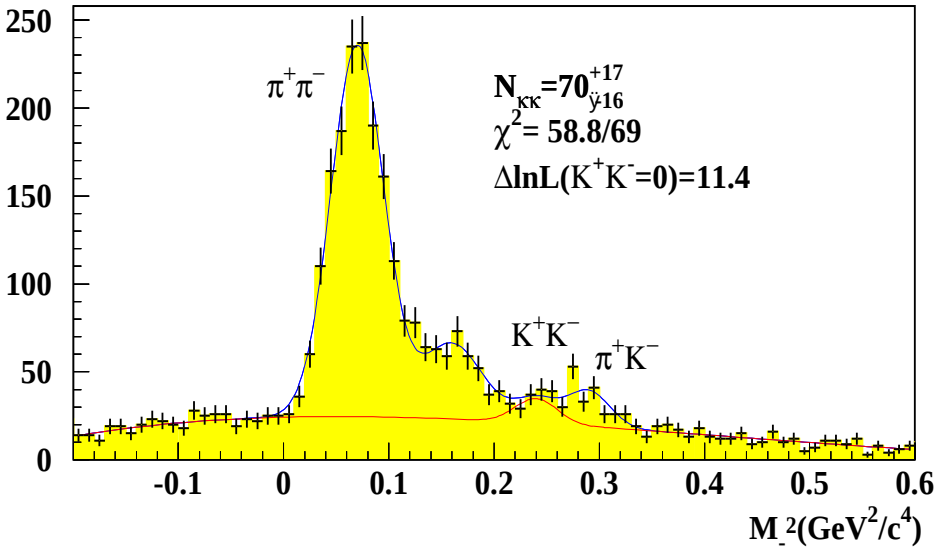

Fig. 15. *Spectrum of squared negative mass M_-^2 measured with Vertical Hodoscopes under K^+ mass hypothesis, for the complete 2001,2002 and 2003 $p-Ni$ data sample with Lambda triggers. The maximum likekyhood fit is explained in the text. The significance of the K^+K^- signal at average pair momentum $p = 4.8GeV/c$ is indicated.*

Table 3
Parameter setting in maximum likekyhood fit to M_-^2 spectrum.

Parameter	Value
$x^0{}_{\pi\pi}$	0.07
$x^0{}_{KK}$	0.24
$x^0{}_{\pi K}$	0.29
$x^0{}_b$	0.16
σ_{KK}	0.02
$\sigma_{\pi K}$	0.02

Parameter	Value
$\sigma_{\pi\pi}$	0.025
σ_b	0.029
$A_{\pi\pi}$	1327.2
A_{KK}	79.9
$A_{\pi K}$	101.8
A_b	311.8

Parameter	Value
B	1449.2
$c0$	0.5978
$c1$	0.3687
$c2$	-3.9717
$c3$	4.3075
$c4$	-1.3526

whereas for N_{KK} both the positive (see Fig. 13 center) and negative mass cuts are subject to independent efficiency corrections. In the latter case a 6-fold product of efficiency factors was taken into account (see Fig. 14 and Table 2). The final numbers are:

$$N_{KK} = N_{KK}^{obs} \times \frac{1}{Eff(K^+)} \times \frac{1}{Eff(K^-)} = 70 \times \frac{1}{0.6303} \times \frac{1}{0.5409} = 205(8)$$

so the measured contamination fraction at 4.8 GeV/c is:

$$r_{KK} = \frac{N_{KK}}{N_{\pi\pi}} = \frac{205}{35219} = 5.8 \times 10^{-3} \tag{9}$$

2.1 Comparison with UrQMD Monte Carlo

The r_{KK} ratio we have obtained at the average momentum $p = 4.8\ GeV/c$ can be compared with our measurement at $p = 2.9\ GeV/c$ using normal physics runs with 2001 data [3] and see whether the evolution of K^+K^- cross-section is well described by the UrQMD Monte Carlo.

In fact, this is the main purpose of this note, because if the experimental data follow this model, it means we can rely on it to perform an accurate correction to Pionium lifetime measurement.

In order to make the comparison as accurate as we can, we need to take into consideration the Coulomb interaction. First of all, we notice that UrQMD does not contain this effect, only relevant at very small values of Q.

Concerning the experimental data , it should be noted that because of the different trigger structure and cuts in the analysis at $p = 2.9\ GeV/c$ and that at $p = 4.8\ GeV/c$, the Coulomb interaction has a different magnitude in each case, which is true for both K^+K^- and $\pi^+\pi^-$ pairs. Moreover, in the standard analysis of Pionium lifetime, the cuts are again different from the ones above.

For a given kinematical configuration Ω, we define the average value of the Coulomb enhancement for $a = \pi\pi, KK$ pair production cross-section as :

$$C_a = \frac{\int_\Omega A_C(Q)(\frac{d\sigma^a}{d^3Q})d^3Q}{\int_\Omega (\frac{d\sigma^a}{d^3Q})d^3Q} = < A_C(Q) >$$

where $A_C(Q)$ is the corresponding Sakharov factor. Concerning the kinematical domain Ω, we have defined three different cases of interest, namely:

A) $1.31 < p_{+-}(GeV/c) < 1.50$

B) $Q_T < 5MeV/c$ and $Q_L < 22MeV/c$

C) $Q_T < 5MeV/c$ and $Q_L < 16MeV/c$

The first (A) corresponds to the analysis at $p = 2.9\ GeV/c$ [3], whereas (B) and (C) correspond to two typical versions of the standard Pionium lifetime analysis [4].

The correction factors obtained for the previous cuts are indicated in table 4, having in mind the following remarks:

a) the cuts indicated above are allways applied to Q-values evaluated in the $\pi\pi$ hypothesis, which is the one implied by ARIANE reconstruction.

b) in the case of asymmetric triggers, the average Q-values are so large ($< Q >= 130 MeV/c$ and $< Q >= 400 MeV/c$ in the $\pi^+\pi^-$ and K^+K^- mass hypothesis respectively) that the Coulomb correction factor is negligible for both $\pi\pi$ and KK.

With the help of table 4, we have plotted the evolution of the ratio r_K as function of the lab-frame momentum p of the pair, taking into account Coulomb corrections. For the sake of reference, we have chosen the configuration that corresponds to the standard Pionium lifetime analysis (cuts C above), and used the correction factors $R_C/R_A = 0.88$ at 2.9 GeV/c and $R_C = 1.29$ at 4.8 GeV/c.

Table 4
Coulomb correction factors for the kinematical cuts A, B and C defined in the text for K^+K^- and $\pi^+\pi^-$ production. Last column shows the ratios $R = C_{KK}/C_{\pi\pi}$.

cuts	C_{KK}	$C_{\pi\pi}$	R
A	2.38	1.63	1.46
B	1.79	1.45	1.24
C	2.00	1.56	1.29

The prediction of UrQMD Monte Carlo was evaluated by running 2049 million p-Ni events from the generator and selecting K^+K^- and $\pi^+\pi^-$ pairs with the cuts: $4.5^o < \theta < 7.0^o$, 1.3 $GeV/c < p_{+-} < 5.0$ GeV/c and $Q < 30 MeV/c$ in the $\pi\pi$ hypothesis, where θ is the angle between the vector sum of the particle momenta and the incoming proton direction and p_{+-} is the momentum of positive or negative particle. The uncorrected curve was multiplied by an acceptance efficiency function determined separately after GEANT-DIRAC processing of K^+K^- pairs, in order to take into account the $K^\pm$ lifetime effect in spectrometer acceptance.

The UrQMD Monte Carlo prediction can be appreciated in Figure 16 as a dotted line. At 2.9 GeV/c the r_{KK} ratio comes out 0.56 (after Coulomb correction), which is larger than the experimental value by a factor 2.7. We have however normalized the Monte Carlo to the experimental value at 2.9 GeV/c. We then see that very good agreement is found with respect to the data measured at 4.8 GeV/c.

Similarly to the case studied for $K^{\pm}\pi^{\mp}$ in the previous section, it seems that UrQMD describes correctly the cross-section dependence on the lab-frame momentum, although the magnitude of the strangeness ratio r_K is not reproduced correctly.

In conclusion, we find that the contamination fractions relevant for Pionium analysis are:

$$\frac{N_{KK}}{N_{\pi\pi}} = 5.8 \times 10^{-3} \times 1.23 = 7.2 \times 10^{-3} \tag{10}$$

at 4.8 GeV/c based upon the UrQMD Monte Carlo extrapolation, in agreement with the experimental data, and

$$\frac{N_{KK}}{N_{\pi\pi}} = 2.38 \times 10^{-3} \times 0.845 = 2.0 \times 10^{-3} \tag{11}$$

at 2.9 GeV/c, according to the Coulomb-corrected experimental measurement.

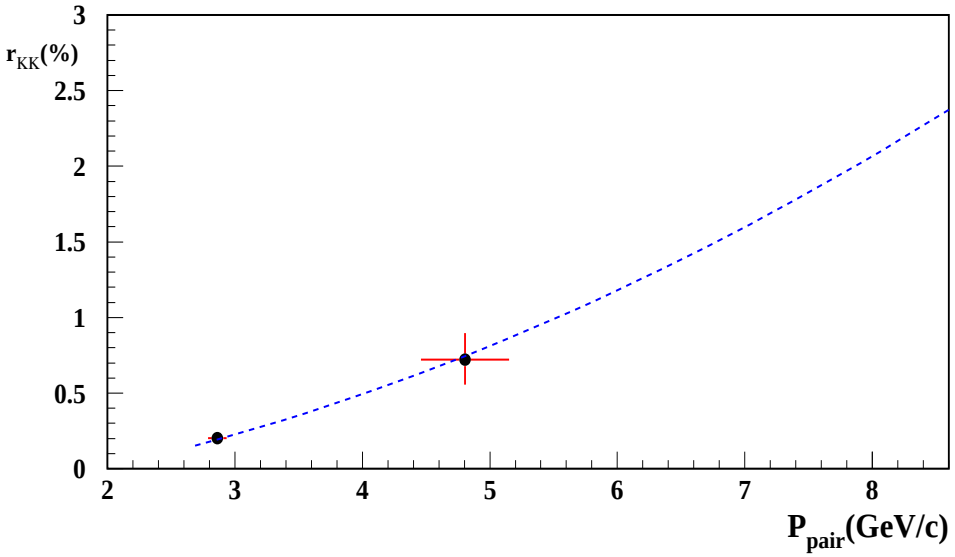

Fig. 16. *Experimental measurements by DIRAC of the $K^+K^-/\pi^+\pi^-$ ratio r_{KK} at two different values of the average pair momentum, namely 2.9 GeV/c and 4.8 GeV/c. The UrQMD Monte Carlo prediction is shown as the dotted line, multiplied by a factor 0.37.*

2.2 The K^-p signal

The presence of a K^-p signal in the M_-^2 spectrum of Fig. 15 can only be unambiguously established when the analysis is made with the correct proton hypothesis for the positive track, rather than the K^+ hypothesis. When this is done, for the particular cuts applied in Fig. 15, no significant signal appears at $M_-^2 = M_K^2$. But indeed these cuts are not appropriate to search for K^-p, since a proton veto has been applied by means of the requirement $-0.2 < m_+^2 < 0.5\ GeV^2/c^4$. When this cut in turned into $m_+^2 > 0.7\ GeV^2/c^4$, in order to enhance the proton yield, a clear K^-p signal shows up, as it can be seen in Fig. 17. Having demostrated the signal [2] , we did not proceed further to a precise determination of the acceptance, since our main interest in this note is the K^+K^-.

It is worth to note that, as a consequence of the combined effect of negative and positive upstream mass cuts, a bias is produced in the M_-^2 distribution which causes an enhancement in the region $M_-^2 \approx 0.125\ GeV^2/c^4$, well appreciated in Fig. 17. We have verified that such characteristic enhancement is actually the origin of the broad structure seen in Fig. 15 at $M_-^2 \approx 0.160\ GeV^2/c^4$, after taking into account the difference in mass hypothesis and upstream mass cuts. This background actually overwhelms the genuin K^-p signal in Fig. 15 which would otherwise be located at the same M_-^2 value.

For the sake of completeness, we also show in Fig. 18 the M_-^2 spectrum with the π^+ hypothesis, showing the π^+K^- and $\pi^+\pi^-$ signals with improved resolution. The cut $m_+^2 < 0.0\ GeV^2/c^4$ was used in this case, in order to suppress both the K^+ and proton yields (according to Fig. 13).

[2] the complete statistics of 2001, 2002 and 2003 p-Ni data from Lambda triggers was used

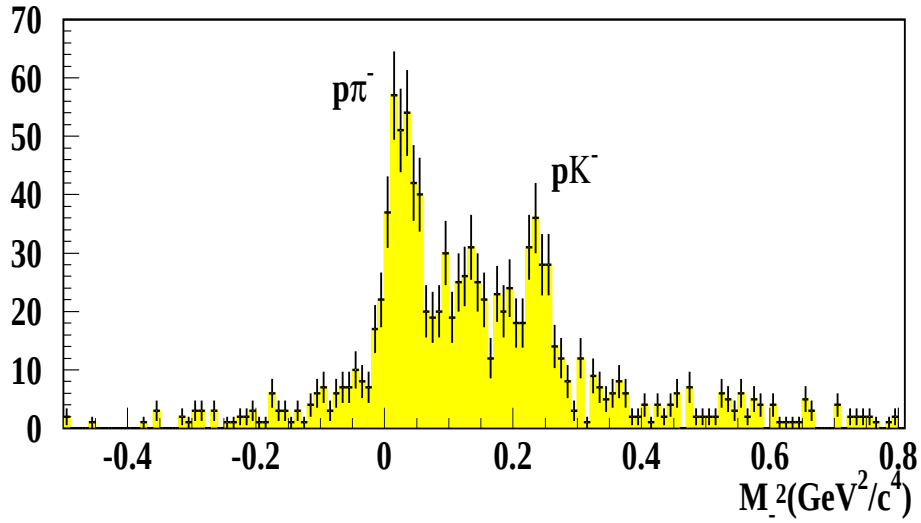

Fig. 17. *Spectrum of squared negative mass M_-^2 measured with Vertical Hodoscopes under proton mass hypothesis. The same data as in Fig. 15, other than the cut $m_+^2 > 0.7\ GeV^2/c^4$.*

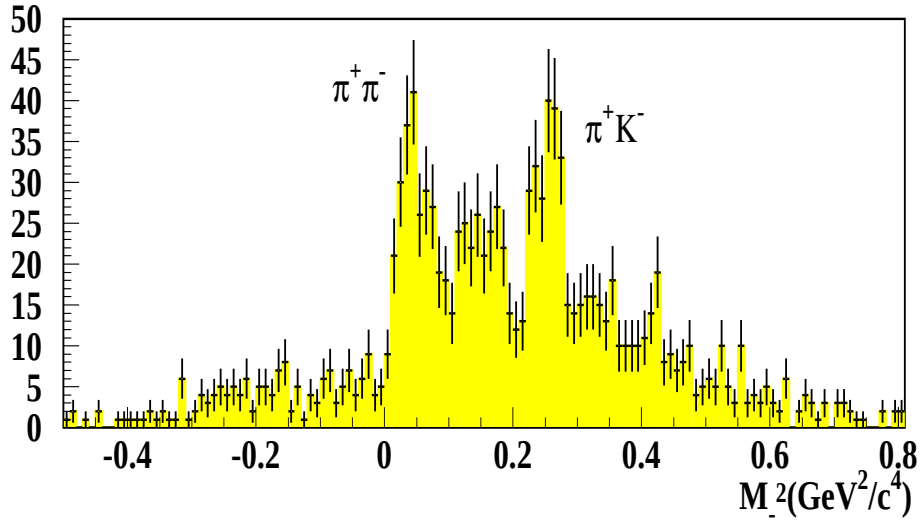

Fig. 18. *Spectrum of squared negative mass M_-^2 measured with Vertical Hodoscopes under π^+ mass hypothesis. The same data as in Fig. 15, other than the cut $m_+^2 < 0.0 GeV^2/c^4$.*

2.3 The K^+K^- signal at 2.9 GeV/c

As part of the analysis presented in this note, we had a closer look at the K^+K^- signal previously observed at 2.9 GeV/c [3], in order to see whether it actually conforms with the strong Coulomb interaction expected in this final state. We selected K^+K^- pairs at very low momentum with the 2001 data (normal physics triggers) by means of the cut $M^2 > 0.2\ GeV^2/c^4$, where M^2 is the improved squared mass determined using all upstream detectors (see selection details in [3]). The Q-value was determined in the K^+K^- hypothesis, and it is shown in Fig. 19, along with the Monte Carlo prediction after the DIRAC standard generator, including the K^+K^- Sakharov factor, processed through the complete simulation/reconstruction chain, and further momentum-selected selected by the cut $1.31\ GeV/c < p_{+-} < 1.50 GeV/c$. Good agreement is observed, although statistical errors are probably too large to make a precise discrimination of the details of the Coulomb interaction.

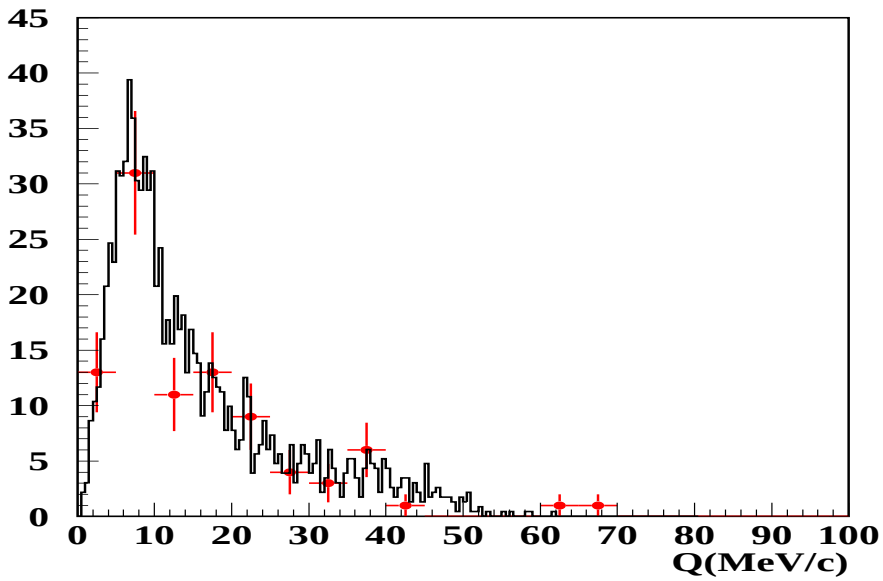

Fig. 19. *Q-spectrum of the K^+K^- sample found in the analysis at 2.9 GeV/c, evaluated under the K^+K^- mass hypothesis (red crosses), compared with full Monte Carlo simulation including Coulomb interaction (continuous line).*

3 Summary and conclusions

A detailed analysis has been done of the pair momentum dependence of the ratios $K^{\pm}\pi^{\mp}/\pi^{+}\pi^{-}$ and $K^{+}K^{-}/\pi^{+}\pi^{-}$ in DIRAC. As far as the momentum derivative is concerned, very good agreement is found with the UrQMD Monte Carlo in both cases. The integrated yields are however at variance with UrQMD, and the corresponding factors have been given. These results provide a good ground for using this Monte Carlo to exprapolate the measured $K^{+}K^{-}$ contamination at $p = 2.9\ GeV/c$ to higher values of momentum, in order to perform an accurate correction for the measurement of Pionium lifetime.

4 Acknowledgements

We would like to give special thanks to the Centro de Supercomputación de Galicia (CESGA), and particularly to the SVGD cluster operators, for their essential and invaluable computing support.

References

[1] UrQMD manual. http://th.physik.uni-frankfurt.de/~ urqmd/
M. Bleicher et al., J. Phys. G25 (1999) 1859; hep-ph/9909407.

[2] B. Adeva et al., The time-of-flight detector of the DIRAC experiment, Nucl. Instr. Meth. A491 (2002) 41.

[3] DIRAC note 06-05 : Experimental Measurement of a $K^{+}K^{-}$ Signal at $p = 2.9GeV/c$ in Ni 2001 Data, B. Adeva, A. Romero and O. Vázquez Doce.

[4] DIRAC Note 06-03: Measurement of pionium lifetime, B.Adeva, A.Romero, O.Vazquez Doce.

[5] Nucl. Instr. Meth. A491 (2002) 376. [hep-ex/0202045]

[6] DIRAC note 04-06 : Experimental determination of momentum resolution in DIRAC using Lambda events, B. Adeva, A. Romero and O. Vázquez Doce.

[7] DIRAC Note 02-09: New ionization hodoscope: design and characteristics, V. Brekhovskikh, M. Jabitski, A. Kuptsov, V. Lapshin, V. Rykalin, L. Tauscher.